ABE 30

APPENDIX

Development of a 0.5 Tesla Permanent Conical Magnet

BY

MANLIO G. ABELE

June, 2003
New York, N.Y.
© Copyright Manlio G. Abele 2003

Contents

1. Introduction 3
2. Conical Magnet 3
3.Design Considerations 19
4. Compensation of Field Distortion 23
5. References 34

1. INTRODUCTION

The generation of highly uniform magnetic fields is the primary goal of the design of magnets for NMR imaging in medical applications. The magnet described in this paper is a novel structure of permanently magnetized material that extends the field range to 0.5 Tesla, well above the current limit of commercially available permanent magnets, with a design approach that is consistent with size and weight well within practical limits.

The magnet combines a conical structure of permanently magnetized material with ferromagnetic pole pieces. The geometry of the magnet is computed in Section 2, that presents the principle of operation and the basic characteristics. The effect of the field perturbation due to the open magnet configuration is discussed in Section 3.

2. CONICAL MAGNET

Fig. 2.1 shows the basic conical structure of magnetized material contained between two coaxial cones of half angles è_1, è_0. The material is assumed to be magnetized with a uniform remanence J_0 parallel to the axis z of the cones. The medium surrounding the external cone is assumed to be non-magnetic, and the medium inside the internal cone is assumed to be a ferromagnetic material with infinite magnetic permeability.

Assume a system of spherical coordinates ñ, è, ø where ñ is the distance of a point from the center O of the cones, è is the angle between ñ and the axis z of the cones, and ø is the angle between the plane formed by a point P and the z axis and an arbitrary plane that contains the z axis.

The structure of Fig. 2.1 has been analyzed in detail by the author in a Technical Report [1]. Assume the limit of infinite radial dimension of the cones and consider the special case of a field configuration independent of the angular coordinate ø. Let

$$x = \cos \text{è} \qquad (2.1)$$

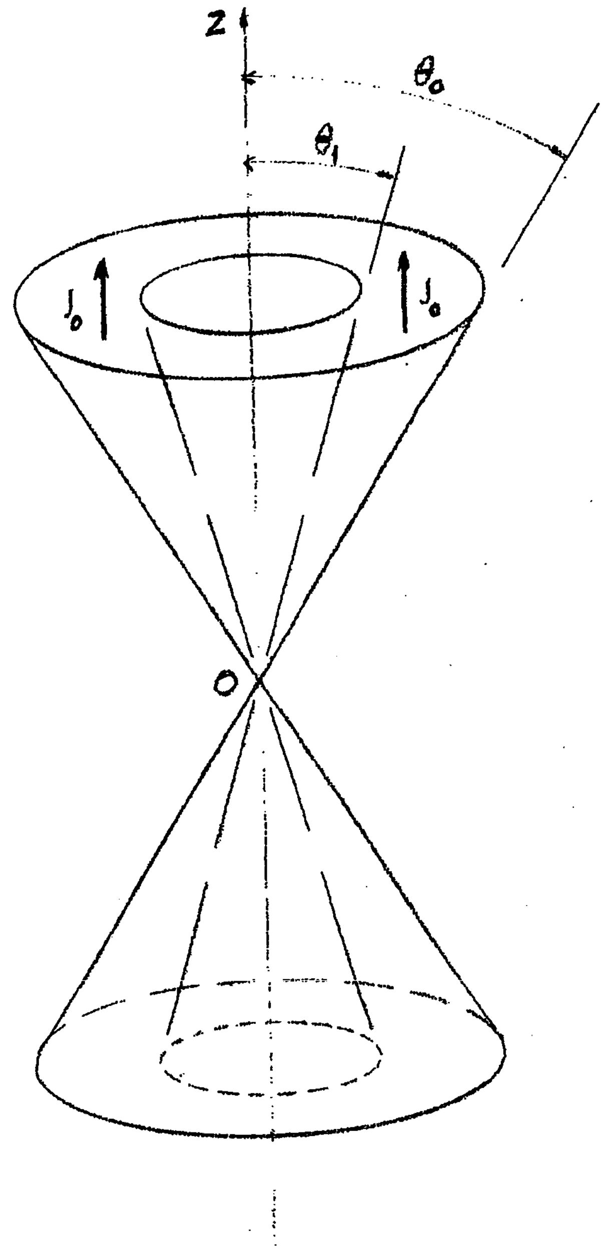

Fig. 2.1 Conical Structure.

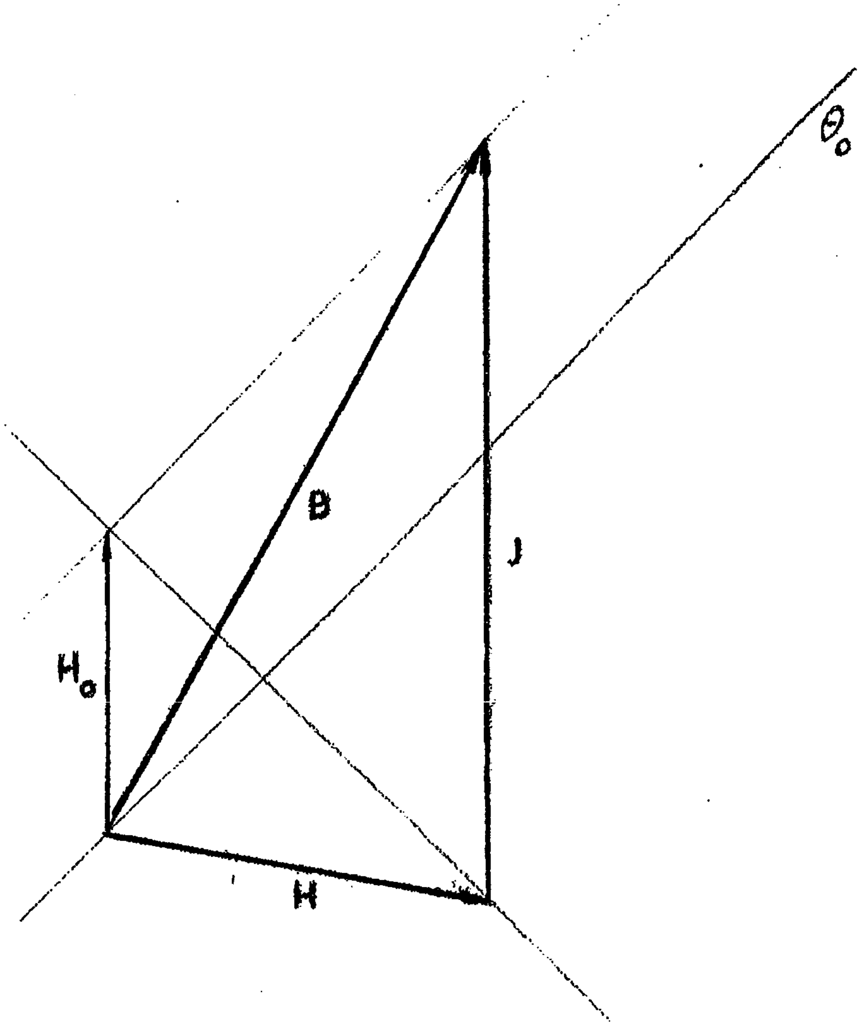

Fig. 2.2 Magnetic induction and intensity at the surface $\theta = \theta_0$.

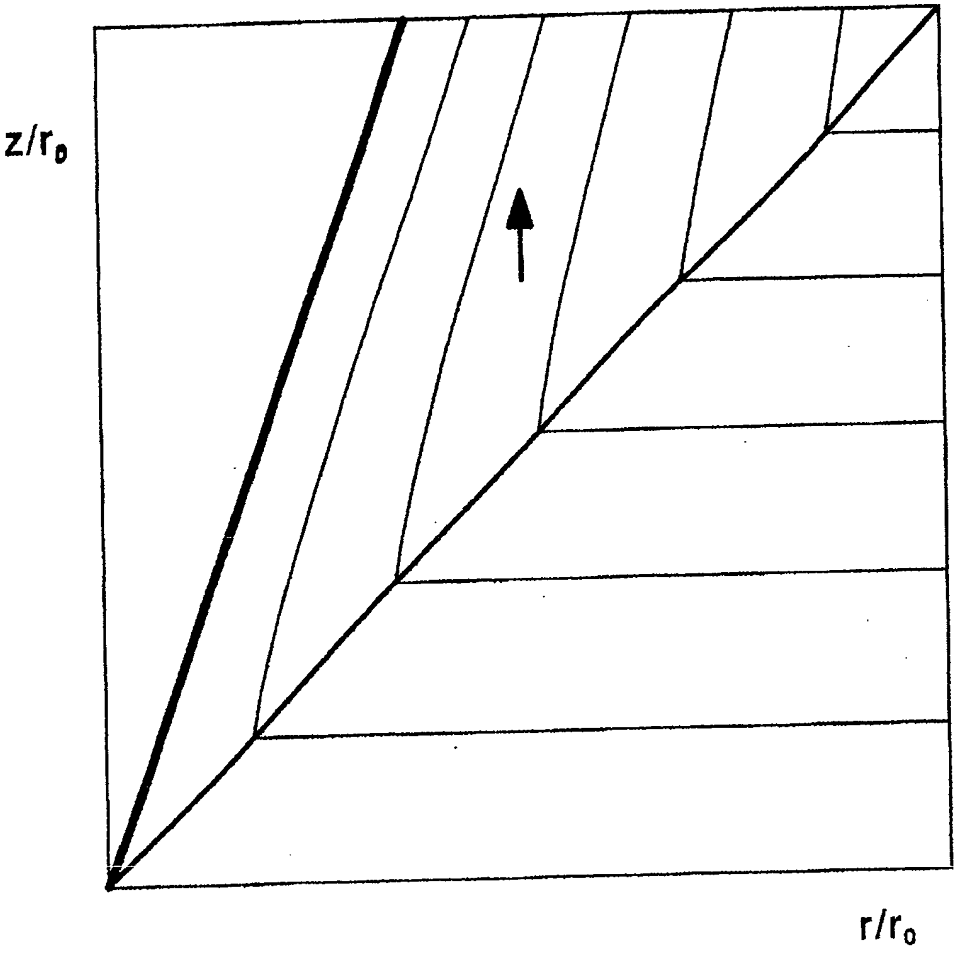

Fig 2.3 Equipotential lines.

The magnetostatic potential Ö (ñ, è) generated by remanence J_0 within the magnetized material is given by the particular solution of the Laplace's equation that satisfies the boundary condition

$$\text{Ö (ñ, è)} = \text{O} \qquad (2.2)$$

One has

$$\varphi(\rho,\theta) = -\frac{J_0}{\mu_0}\left(1-X_0^2\right)X_0\rho\left[1-\frac{X}{X_1}+\frac{X}{2}\ell n\left[\frac{(1+X_1)}{(1-X_1)}\frac{(1-X)}{(1+X)}\right]\right] \qquad (2.3)$$

for $\text{è}_1 < \text{è} < \text{è}_0$ and $\text{ð} - \text{è}_0 < \text{è} < \text{ð} - \text{è}_{1.}$ ì_0 is the magnetic permeability of a vacum and

$$X_0 = \cos \text{è}_0, \; X_1 = \cos \text{è}_1 \qquad (2.4)$$

In the region $\text{è}_0 < \text{è} < \text{ð} - \text{è}_0$ the magnetostatic potential is

$$\phi(\rho,\theta) = -\frac{J_0}{\mu_0}\left(1-x_0^2\right)x\rho\left[1-\frac{x_0}{x_1}+\frac{x_0}{x_2}\ell n\frac{(1+x)}{(1-x_1)}\frac{(1+x_0)}{(1-x_0)}\right] \qquad (2.5)$$

Eq. (2.5) is the potential of a uniform magnetic field of intensity H_0 oriented parallel to the z axis and of magnitude

$$\text{ì}_0 H_0 = K J_0 \qquad (2.6)$$

where

$$K = \left(1-x_0^2\right)\left[1-\frac{x_0}{x_1}+\frac{x_0}{2}\ell n\frac{(1+x_1)(1-x_0)}{(1-x_1)(1+x_0)}\right] \qquad (2.7)$$

The equipotential surfaces are planes perpendicular to z in the region $\text{è}_0 < \text{è} < \text{ð} - \text{è}_0$ and within the magnetized material the equipotential surfaces are given by the equation

$$\rho = \frac{C}{\frac{x}{2}\ell n\frac{(1+x_1)(1-x)}{(1-x_1)(1+x)}+1-\frac{x}{x_1}} \qquad (2.8)$$

where

$$C = \frac{\mu_0 \phi}{J_0 x_0 \left(1 - x_0^2\right)} \qquad (2.9)$$

The field inside the cone is not uniform and the values of H and B at the surface of the cone $è = è_0$ are given by the vector diagram of Fig. 2.2

An example of the equipotential lines given by Eq. (2.8) is shown in Fig. 2.3 for the cone angles $è_1 = 20°$, $è_0 = 45°$. In this example, the uniform field in the region $è_0 < è < ð - è_0$ corresponds to a value of K as given by Eq. (2.7)

$$K = 0.426 \qquad (2.10)$$

Hence if one assumes a value

$$J_0 \sim 1.3 \text{ Tesla} \qquad (2.11)$$

the cone generates a uniform field of intensity H_0

$$ì_0 H_0 \sim .55 \text{ Tesla} \qquad (2.12)$$

The basic schematic of Fig.2.1 can provide the computation of the field in a structure where the magnetized material is eliminated in the region

$$-z_0 < z < +z_0 \qquad (2.13)$$

The new structure is shown in Fig. 2.4 where the two areas of the surfaces that limit region (2.13) are circles of radius

$$r_0 = z_0 \tan è_0 \qquad (2.14)$$

The two circular areas are assumed to be surfaces of an infinite magnetic permeability material. Furthermore, the equipotential surface within the magnetized material that start from the circle of radius r_0 is also assumed to be transformed into a surface of infinite magnetic permeability material. As a consequence, the field configuration inside the magnetized material is still given by Eq. (2.3) and the structure of Fig. 2.4 generates the uniform field defined by Eqs. (2.6),(2.7) everywhere outside the magnetized material, including the gap between the

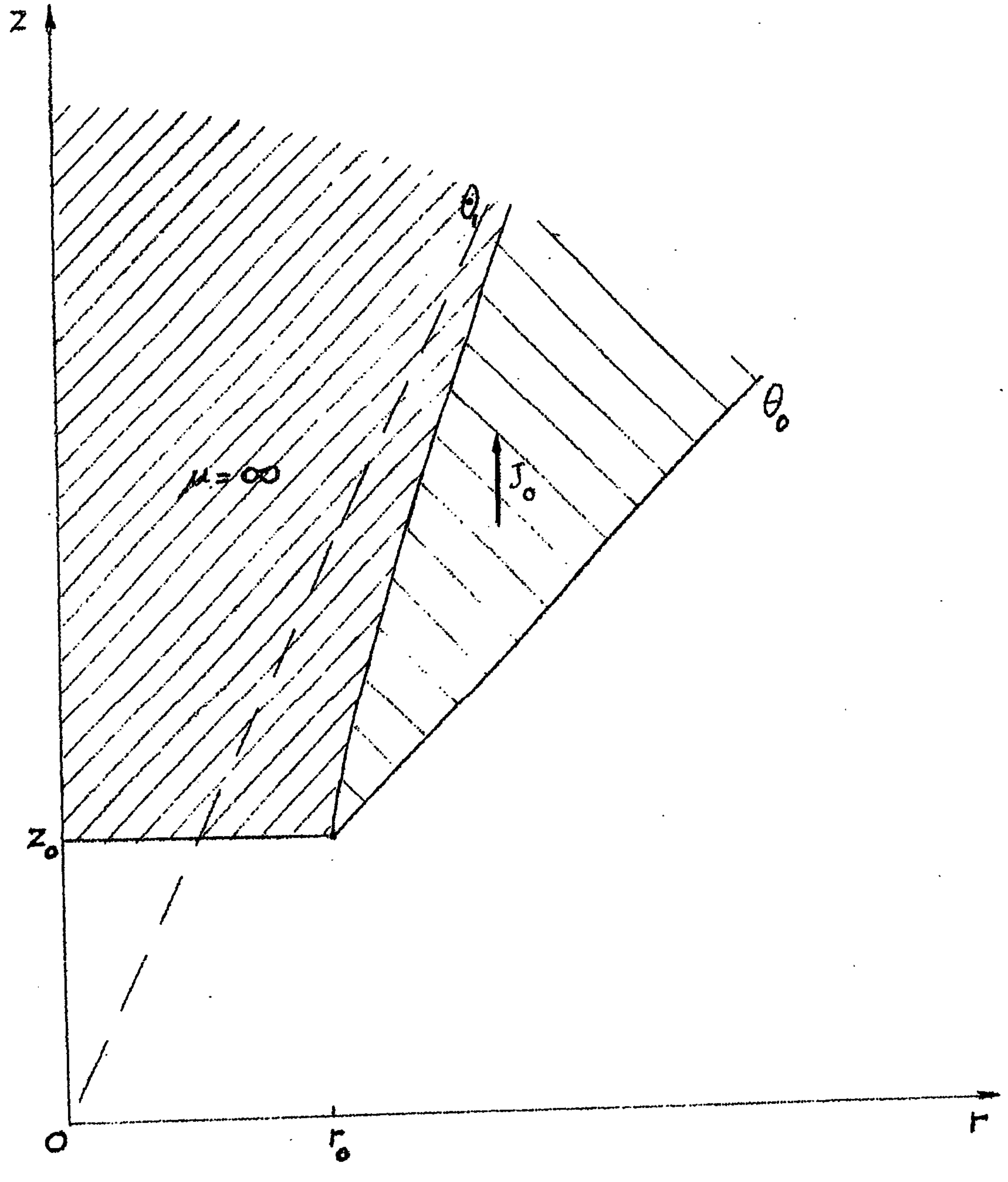

Fig. 2.4 Generation of the central gap.

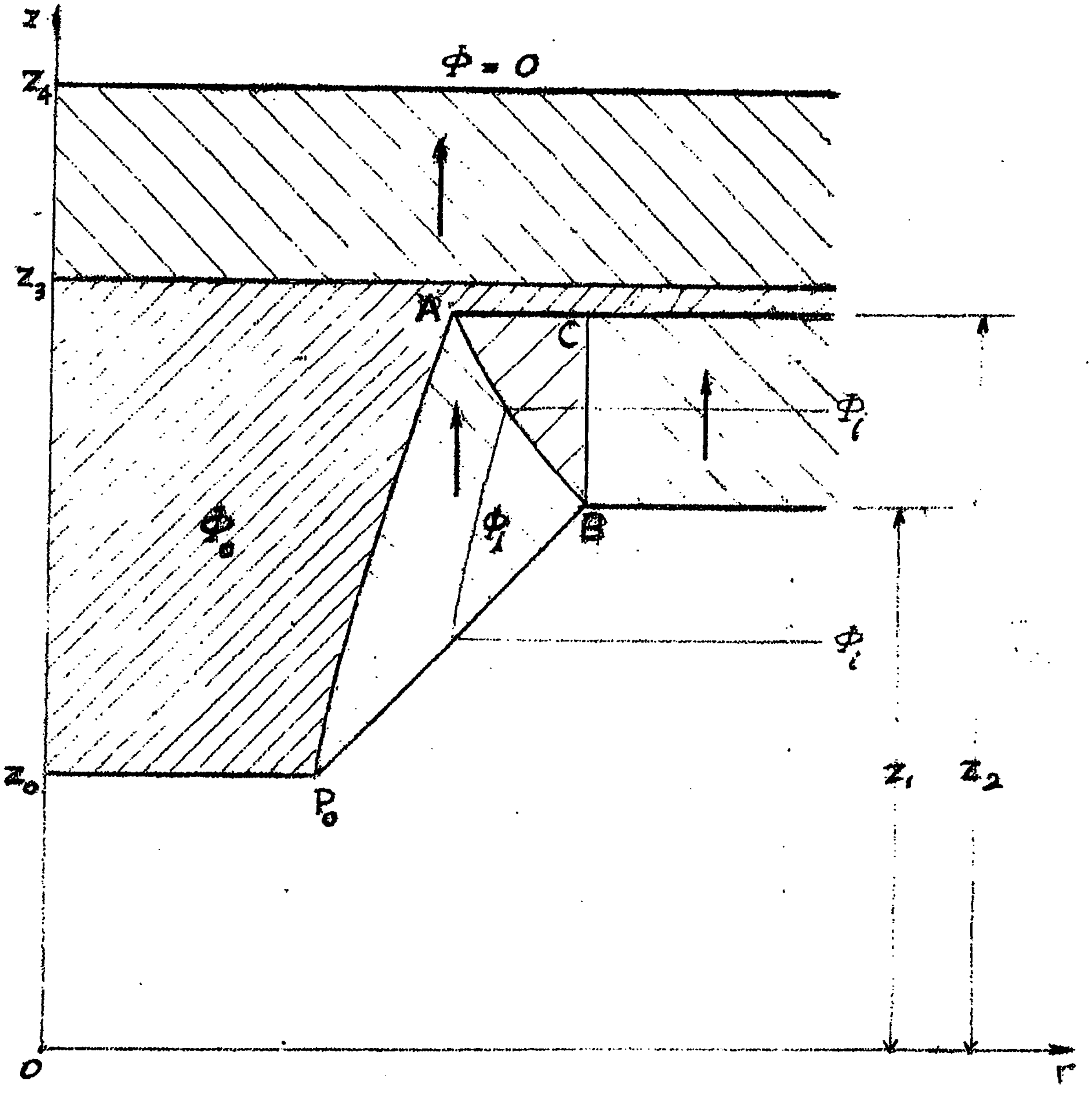

Fig. 2.5 Basic schematic of the magnet.

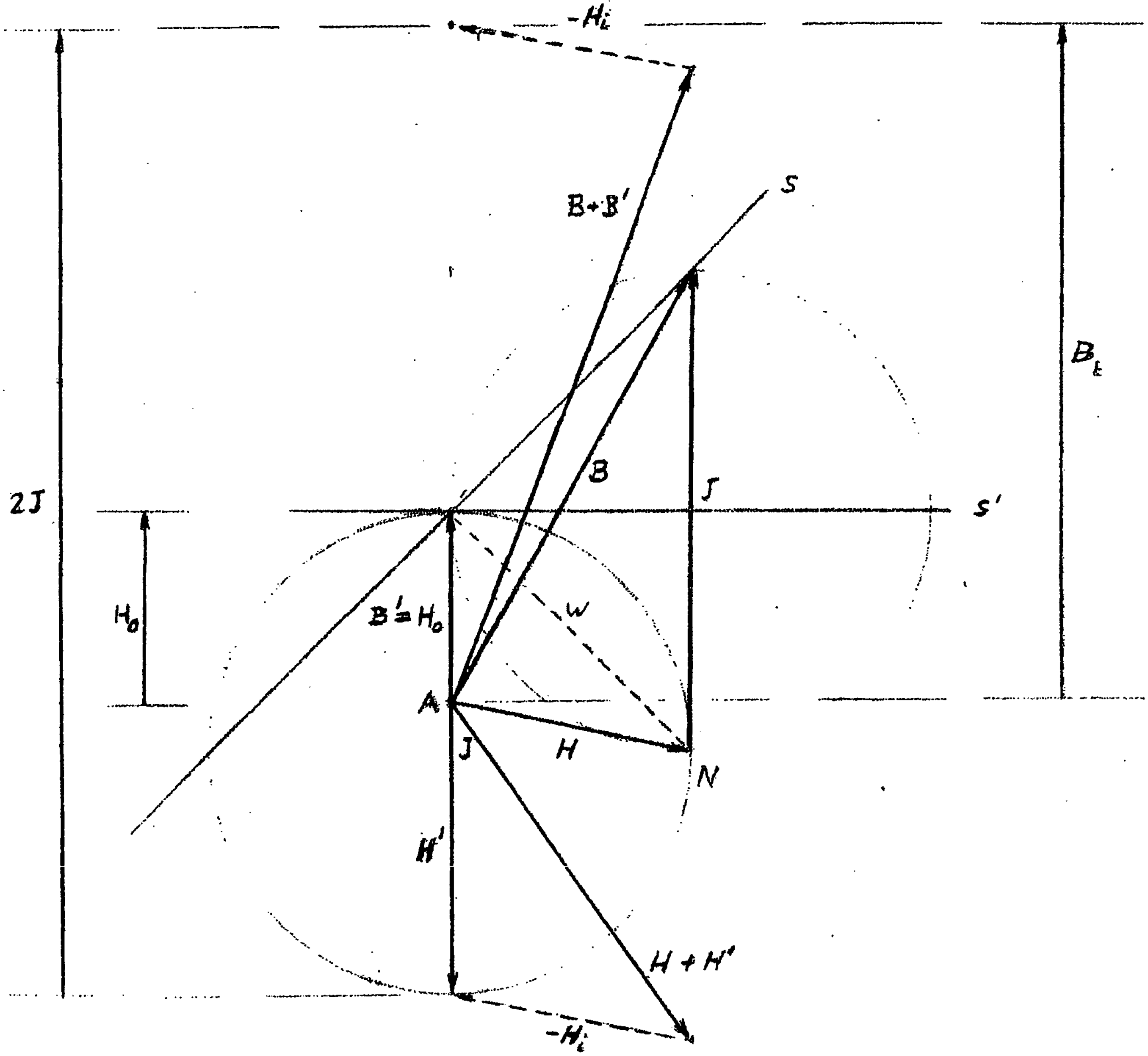

2.6 Computation of the remanence of the transition region (ABC).

ferromagnetic plates of radius r_0. An additional source, other than the magnetized material in Fig. 2.4, is necessary to maintain the block of ferromagnetic material in the structure of Fig 2.4 at the potential

$$\ddot{O}_0 = -H_0 z_0 \qquad (2.15)$$

The design of the complete structure depends upon the external termination of the conical body of magnetized material. This can be accomplished by the transition from the conical structure to a cylindrical structure shown in the schematic of Fig. 2.5. The cylindrical structure is contained between the planes $z = z_1$, $z = z_2$ and its thickness $z_2 - z_1$ is given by

$$K = \frac{Z_2 + Z_1}{Z_2} \qquad (2.16)$$

The cylindrical structure is magnetized with the uniform remanence J_0 parallel to the axis z. The structure cannot interface directly with the cone and a region (ABC) of magnetic material of remanence different from J has to be inserted between the cone and the cylindrical structure, as shown in Fig. 2.5. The computation of the geometry of region (ABC), and its magnetization is complicated by the cylindrical configuration of the magnet. However, even in the approximation of a two-dimensional geometry independent of the coordinate perpendicular to the plane of the section of Fig. 2.5, the transition between the two median would require a uniform remanence oriented along the z axis of magnitude [2]

$$J = 2 J_0 \qquad (2.17)$$

as shown in the vector diagram of Fig. 2.6, where H, B indicate the intensity and the induction in the cone, and H', B' indicate the intensity and the induction in the cylindrical structure. Because the intensity in the transition region coincides with the intensity in the cylindrical region the interface (AB) between the cone and region (ABC) is a line w of the points P of intersection of the equipotential lines Ö in the cone with the same equipotential lines within (ABC).

By virtue of Eqs (2.8) and (2.9), the equation of the equipotential lines inside the cone can be written in the form

$$\frac{\rho}{\rho}=\frac{\frac{x_0}{2}\ell n\frac{(1+x_1)(1-x_0)}{(1-x_1)(1+x_0)}+1-\frac{x_0}{x_1}}{\frac{x}{2}\ell n\frac{(1+x_1)(1-x)}{(1-x_1)(1+x)}+1-\frac{x}{x_1}} \tag{2.18}$$

where ñ is the distance of the point of potential Ö on the cone of angular width $è_0$ from O. In the coordinates ñ, è, the equations of the equipotential lines in the region (ABC) are

$$\rho=\frac{z}{x},\frac{z_2-z}{z_2-z_1}=\frac{\varphi}{\varphi_1} \tag{2.19}$$

Thus, the system of Eqs. (2.18) and (2.19) provides the equation of line w

$$\frac{1}{x}=\frac{\bar{\rho}}{z}\frac{\frac{x_0}{2}\ell n\frac{(1+x_1)(1-x_0)}{(1-x_1)(1+x_0)}+1-\frac{x_0}{x_1}}{\frac{x}{2}\ell n\frac{(1+x_1)(1-x)}{(1-x_1)(1+x)}+1-\frac{x}{x_1}} \tag{2.20}$$

The potential Ö of the ì $=\infty$ component of the magnetic structure of Fig. 2.5 is generated with the additional planar structure contained between the planes $z = z_3$, $z = z_4$ where z_3 can be chosen somewhat arbitrarily, and the thickness $z_4 - z_3$ is given by

$$\frac{z_4-z_3}{z_0+z_4-z_3}=K \tag{2.21}$$

Again, this external planar structure is uniformly magnetized with the remanence J_0 parallel to the z axis. The surface $z = z_4$ is the interface between the magnetic structure and the external yoke of the magnet that closes the flux of the magnetic induction.

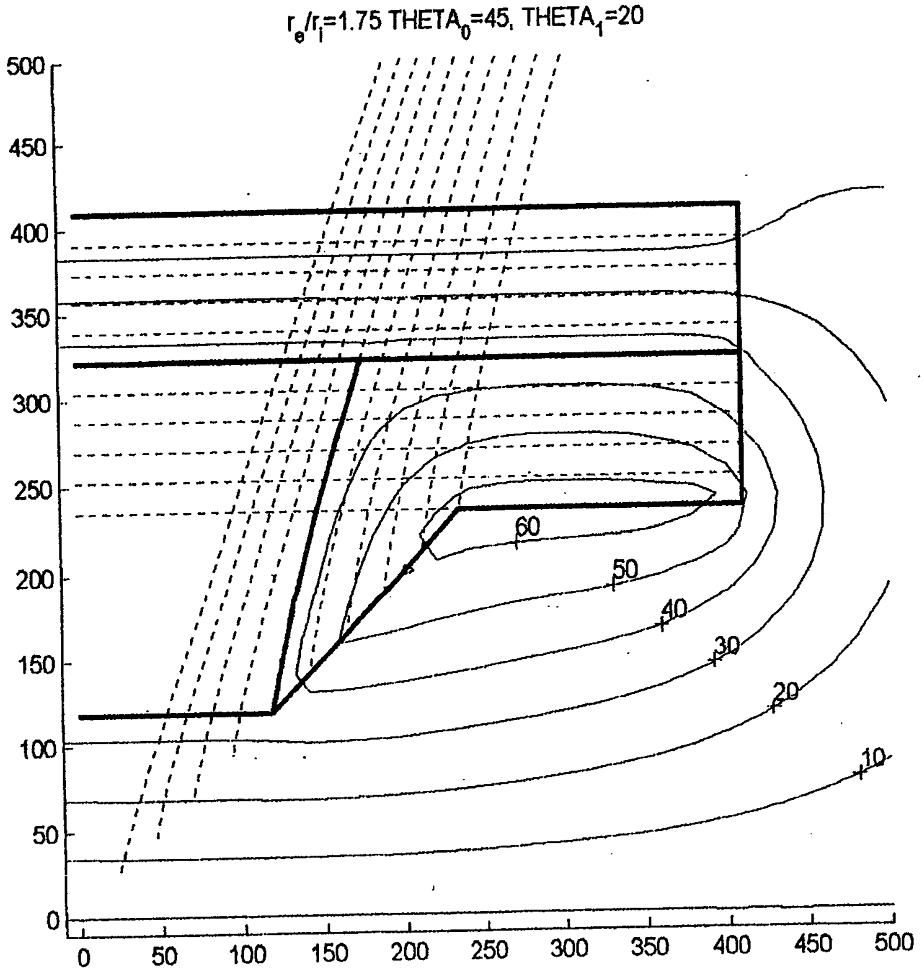

Fig. 3.1 Equipotential lines with no transition structure between cone and cylinder.

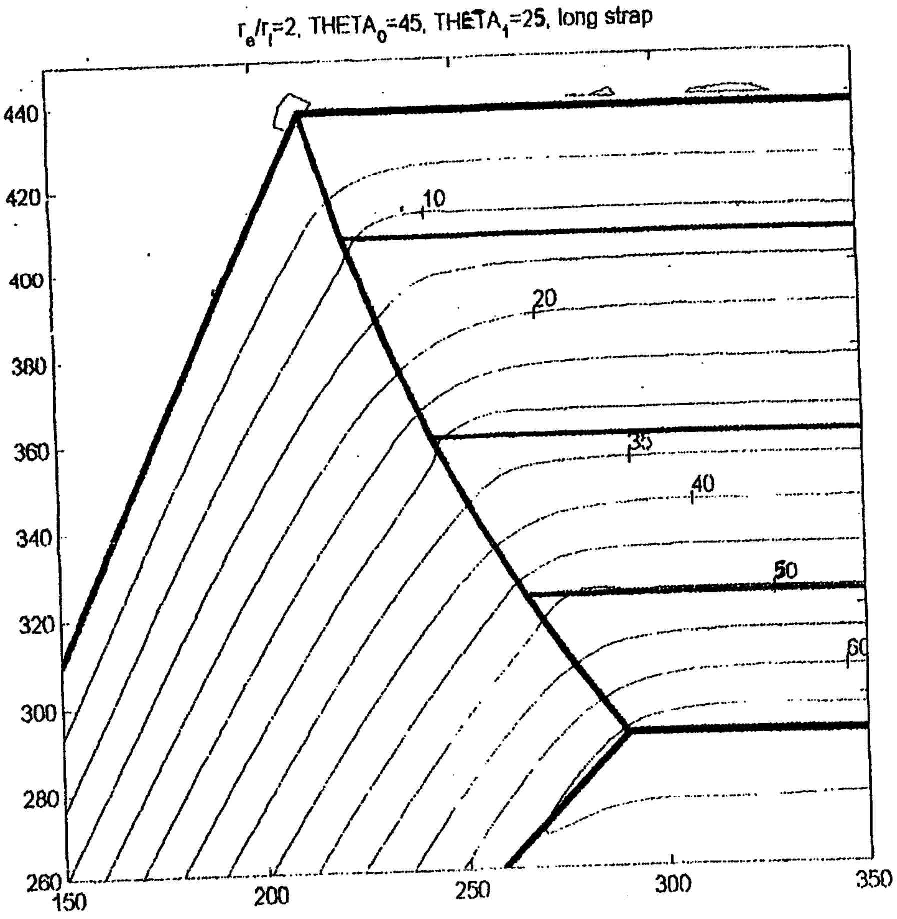

Fig. 3.2 Equipotential lines in the transition region with the insertion of the three straps.

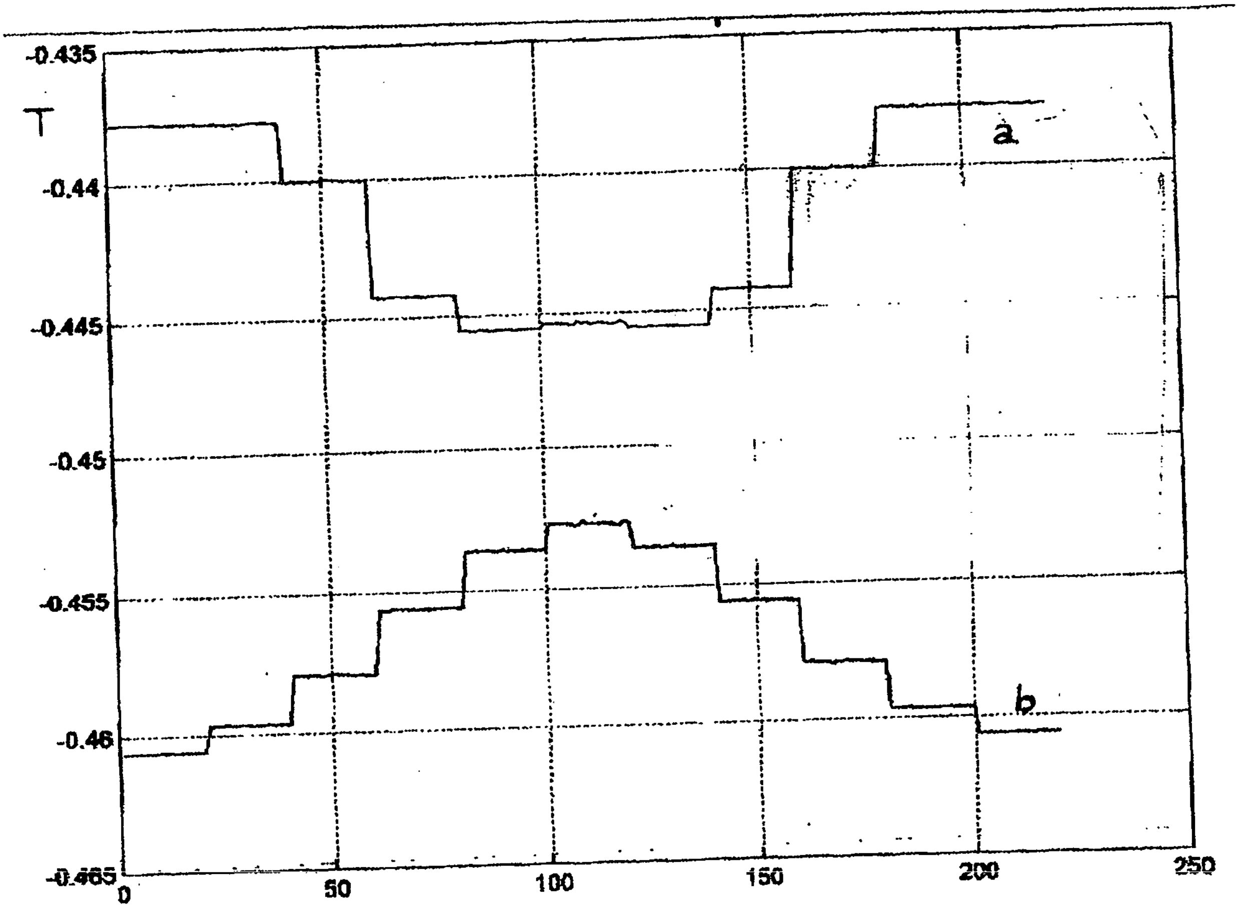

Fig. 3.3 Field on a reference sphere with center at O and diameter $2z_o$. (a) conical magnet. (b) conventional magnet.

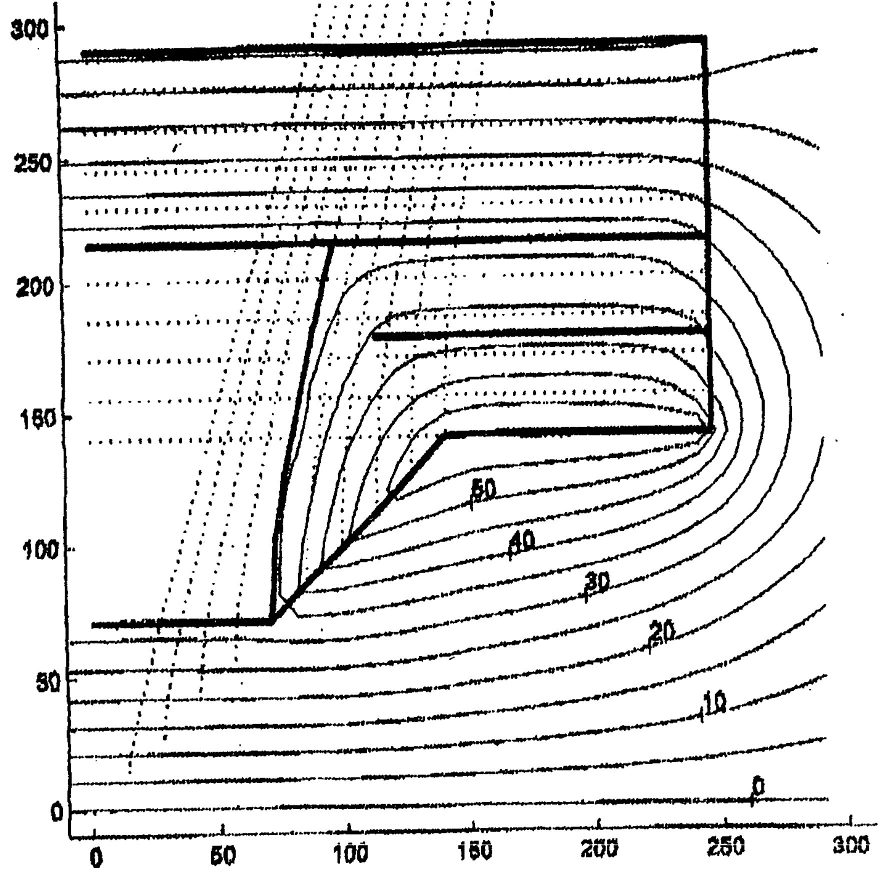

Fig. 3.4 Equipotential lines with a single strap and $K' = 1.03$ K .

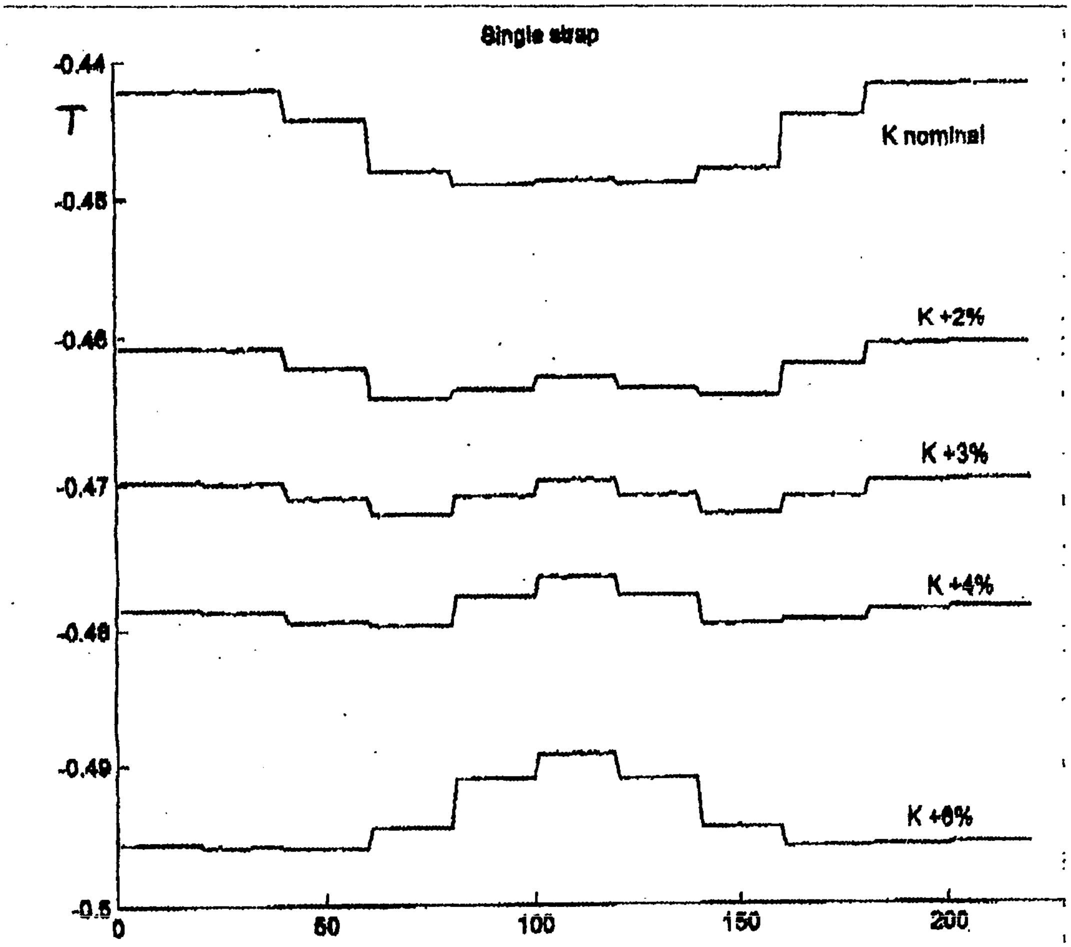

Fig. 3.5 Field over the reference sphere for increasing valuve of K'.

3.DESIGN CONSIDERATIONS

The exact solution presented in Section 2 is affected by two main constraints in its implementation in a practical design. In the first place, a finite external radius has to be chosen and its value has to be large enough to minimize the perturbation of the field uniformity in the gap between the pole pieces. Second, the design presented in this paper is aimed at the development of a magnetic structure capable of generating the largest possible field compatible with practical considerations. This means that the highest commercially available remanence J would be chosen for the magnetic material. If a value $J_0 \sim 1.3$ T is chosen, as assumed in Section 2, no permanent magnet of remanence 2 J_0 is available for the implementation of the exact designs of the transition between the cone and the cylindrical sections. A remanence 2 J_0 is well above the theoretical limit of what can be achieved in the development of rare earth magnetic materials. As a consequence an approximate solution may be adopted taking advantage of the fact that the transition region is well outside the region of interest is the gap between the pole pieces. The approximate solution adopted in this design eliminates the transition region (ABC) and assume a uniform distribution of J_0 throughout the region of the cone and the cylindrical region as shown in Fig. 3.1. The effect of the field distortion is illustrated in the example of Fig. 3.1 which shows the result of the numerical calculation of the equipotential lines. A partial correction of the field distortion in Fig. 3.1 is possible with the insertion of magnetized straps within the transition region. The straps are relatively thin plates of high magnetic permeability material deployed along the theoretical equipotential surfaces within the transition region. Schematically, the insertion of the straps is shown in Fig 3.2 where the straps are extended over the entire radial dimension of the cylindrical structure.

Ideally, the region of interest should extend to the full region of the gap between the pole pieces. Consider the value of the field intensity over a sphere whose center coincides with the center of the gap and whose diameter is equal to the dimension $2z_0$ of the gap. An example of the numerical calculation of the field intensity over circles on the sphere in planes perpendicular to the axis z is shown in Fig. 3.3. One observes that the field at the points $z = \pm z_0$ is lower than the field on the equational plane $z = 0$.

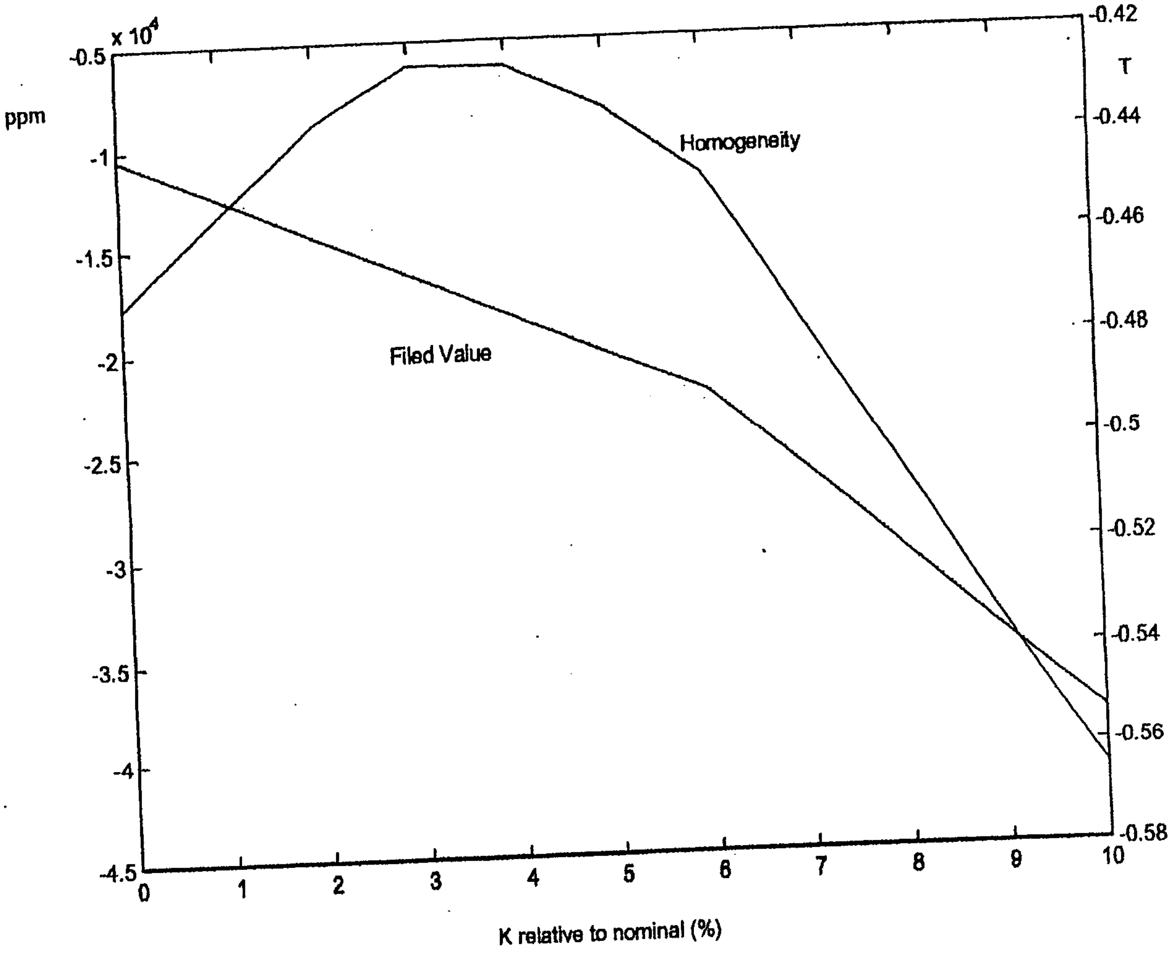

Fig. 3.6 Field homogeneity and field intensity versus K'

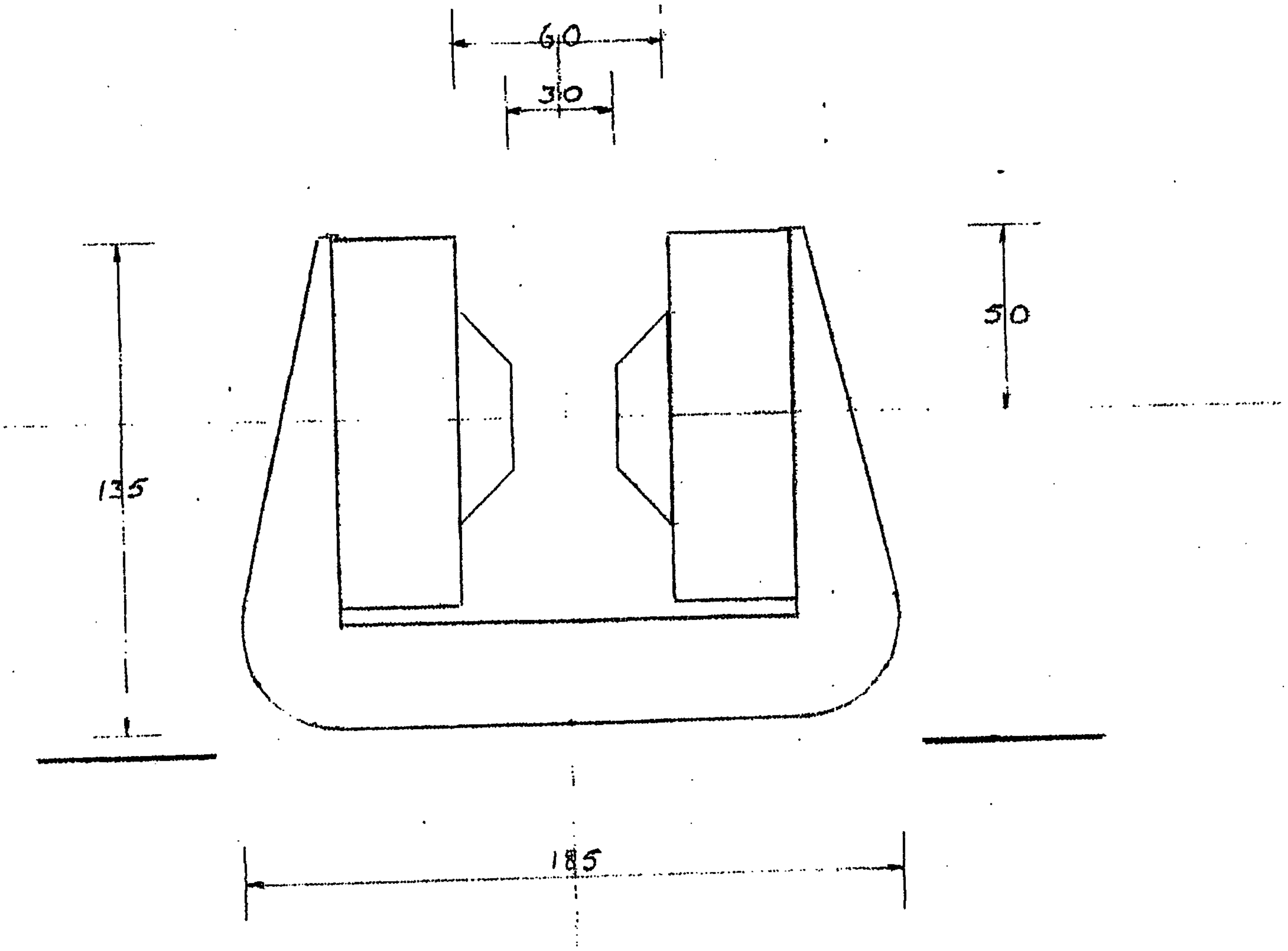

Fig. 3.7 View of the magnet with the external yoke.

This is contrary to what is normally found between the pole pieces of a conventional magnet, where the filed increases from the center along the axis and decreases with the radial distance in the plane perpendicular to the axis as shown in Fig.3.3. Thus, in the implementation of the conical magnet, the field generated by the cylindrical region over compensates the field generated within the central gap. As a consequence, the external planar structure contained between the planes $z_3 < z < z_4$ can be designed for a value $K' > K$ and the value of K' can be chosen to minimize the variation of the field intensity in the region of interest.

The results of the selection of K' are shown in the magnet configuration of Fig 3.4 where a single strap is used for the partical correction of the field distortion in the transition between cone and cylindrical structure. The equipotential lines in Fig 3.4 correspond to

$$K' = 1.03\ K \qquad (3.1)$$

The plotting of the intensity over the reference sphere of diameter approximately equal to $2z_0$ is presented in Fig. 3.5 which shows that for K' larger than the value (3.1) the field intensity on the equatorial plane becomes larger than the intensity on the z axis. At the optimum condition the field homogeneity on the reference sphere is better than ~ 1 %. The homogeneity changes rapidly with different values of K' as shown in Fig. 3.6. As expected, the field intensity within the sphere increases as K' increases. As shown in Fig. 3.5 the field at the center of the sphere is

$$\grave{\imath}_0 H_0 \sim .0.47 \text{ Tesla} \qquad (3.2)$$

for $J_0 \sim 1.38$ Tesla. The homogeneity at condition (3.1) is a remarkably small value as a design parameter of the open magnet presented in this paper, and one can expect the tolerances of fabrication and material properties to have a larger affect on a practical implementation of the design approach. Hence, a conventional shimming technique can be used to improve the homogeneity to a value of the order of 50 ppm or better consistent with imaging requirement.

The schematic of Fig. 3.4 corresponds to the basic parameters

$$K = 0.51,\quad \grave{e}_0 = 45^0,\quad \grave{e}_1 = 16^0$$

$$r_e = 1.75\, r_1 \qquad (3.3)$$

4. COMPENSATION OF FIELD DISTORTION

Assume that the region of interest is the sphere of diameter $2z_0$ and center located at the center O of the magnet, where the field uniformity must satisfy the imaging requirements. A distortion of the uniform field is caused by the finite dimensions of a practical magnet and by the fabrication tolerances of the geometry and distribution of the magnetization. As shown in Section 3, a partial computation of the effect of finite dimensions can be achieved in the design phase by modifying the value of K of the external magnetic structure. The distortion due to the tolerances cannot be compensated in the design phase and requires the use of a shimming technique based on the measurement of the field generated by the assembled magnet. The shimming technique requires the insertion of a magnetic structure whose configuration is dictated by a logic based on the field measurements.

Assume that the shimming is performed by means of a distribution of magnetic dipoles on the conical surface (P_0 B) of the schematic of Fig. 2.5 as shown in Fig. 4.1. The dipole distribution is defined at each point P by a dipole moment density m per unit surface of components m_r, m_z as indicated in Fig. 4.1. Assume that m_r, m_z are independent of the angular coordinate ψ. The dipole distribution m_z on the element of surface $2\pi r d\rho$ of a ring of radius r coaxial with the axis z generates a field on the sphere of radius ρ_0 shown in Fig. 4.2, whose potential is shown in Fig 4.3 for six equally spaced positions on the element of surface line (P_0B) The z component of the intensity corresponding to the six curves of Fig. 4.3 is shown in Fig. 4.4. The effect of the orientation of the dipole moment density is illustrated in Fig. 4.5 where the z component of the intensity is computed for the component m_r of the dipole moment density. The fields generated by m_r, and m_z exhibit a similar behavior. In both cases the field on the reference sphere decreases rapidly with the distance from point P_0. The significant difference between the two cases is the larger intensity generated by m_r located in proximity of P_0 where m_r is essentially perpendicular to the surface of the ferromagnetic pole piece.

Assume that the chosen dipole distribution is limited to the component m_r. The z component of the intensity on the reference sphere of radius ρ_0 can be written in the form

$$\mu_0 H_z(\theta) = \int_{P_0}^{P_1} \Psi(\rho,\theta) m_r(\rho) d\rho \tag{4.1}$$

Where $\psi(\rho,\theta)$ is a function of the geometry of the magnetic structure and the distance between a point of the reference sphere of coordinates θ ψ and a point of the conical surface $\theta = \theta_0$ with the same angular coordinate ψ. The complexity of the geometry of the magnetic structure makes it impossible to achieve an exact analytical solution of Eq. (4.1) and numerical calculations have to be used to map function ψ as a function of θ for each value of ρ. The maximum range of interval P_0P_1 in Eq. (4.1) extends to the length P_0B of Fig 2.5. With the assumption that the dipole distribution in confined to n+1 rings equally spaced alone the radial coordinate ρ at a distance

$$\delta\rho = \frac{\rho_n - \rho_0}{n} \tag{4.2}$$

Eq. 4.1 transforms to

$$\mu_0 H_z(\theta) = \sum_{h=o}^{n} \Psi(\rho_h, \theta) p(\rho_h) \tag{4.3}$$

where

$$p(\rho_h) = m_r(\rho_h)\,\delta\rho \tag{4.4}$$

ρ_0, ρ_n are the radial coordinates of points P_0,B respectively. The field on the reference sphere can be expanded in spherical harmonicics

$$\mu_0 H_z(\theta) = \sum_{k=0}^{\infty} b_k P_k(\cos\theta) \tag{4.5}$$

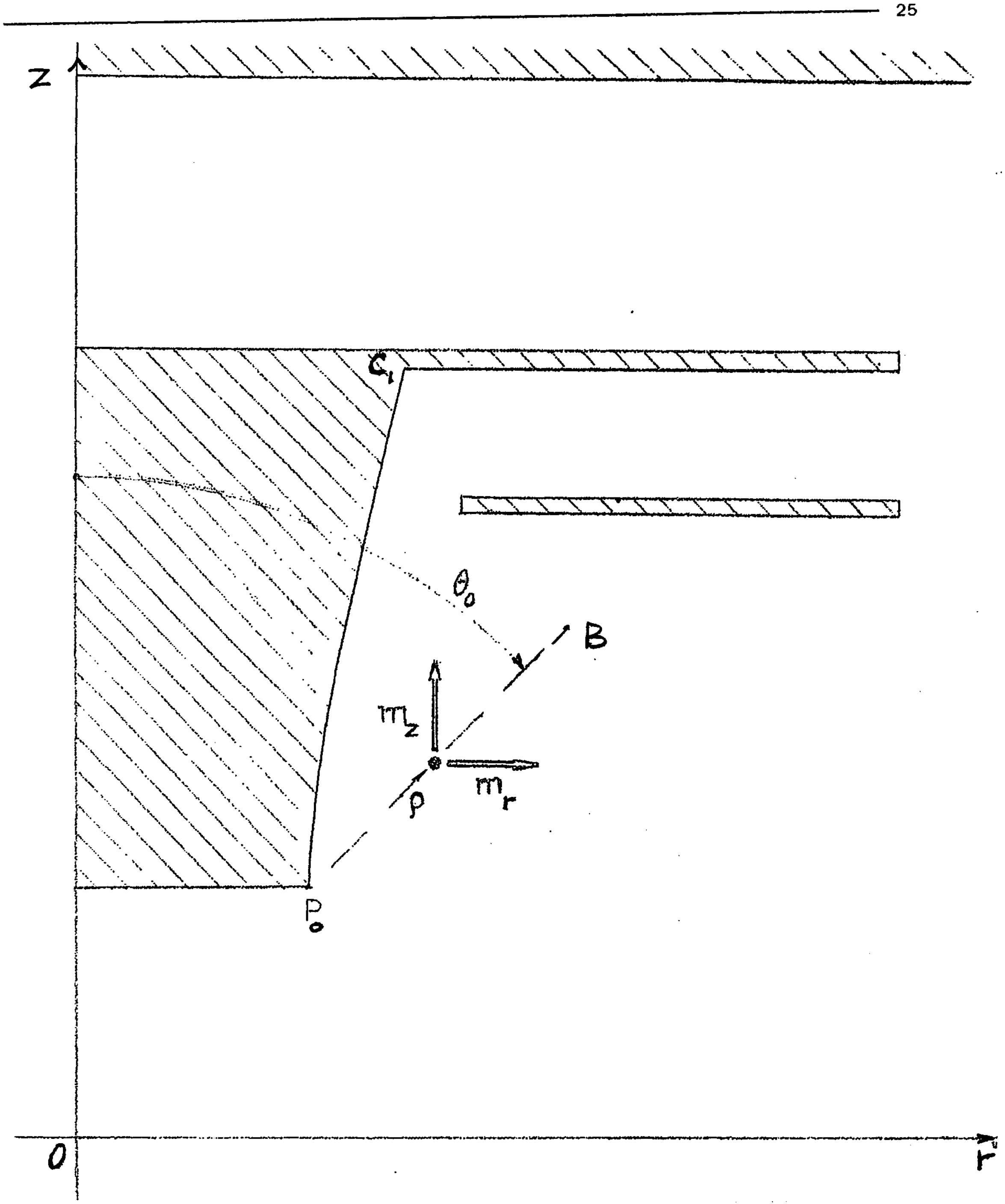

Fig. 4.1 Compensating dipole

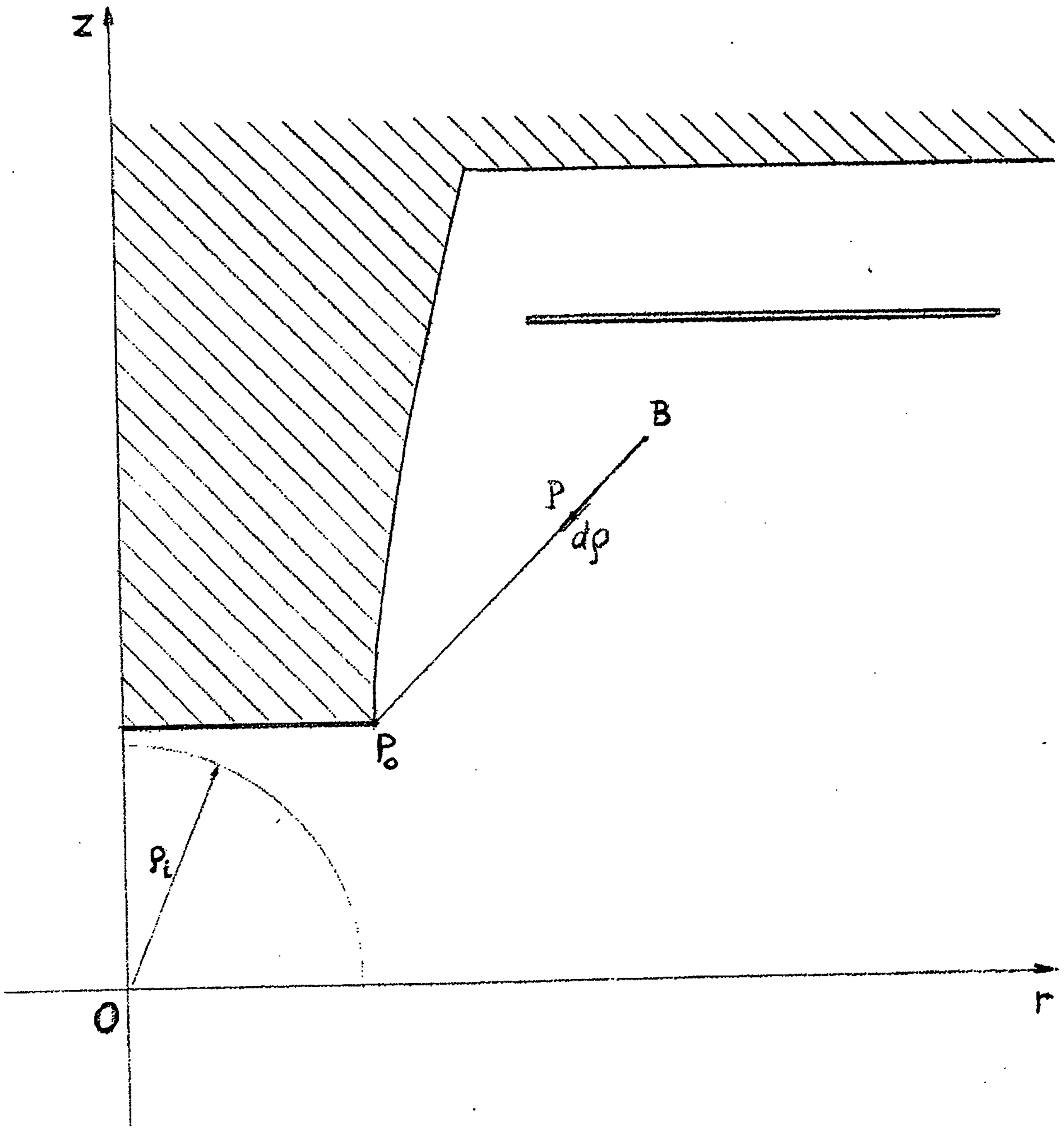

4.2 Schematic for the computation of the dipole field

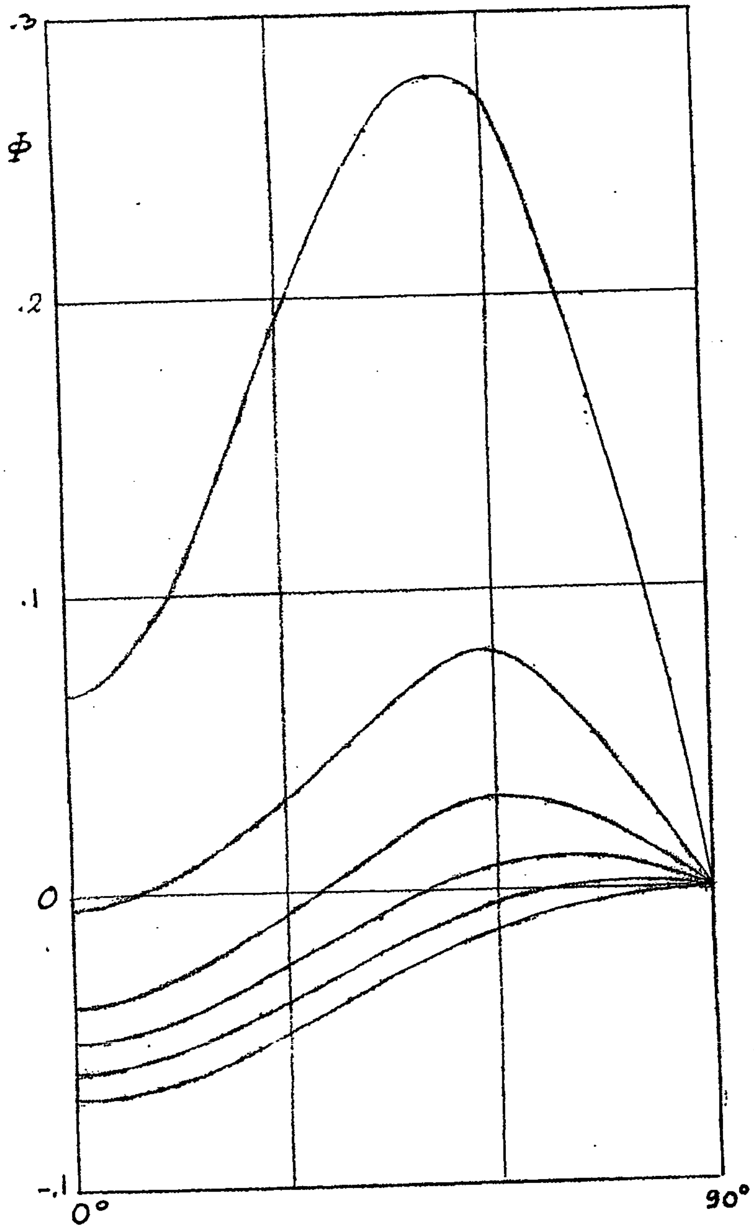

Fig. 4.3 Potential on the reference sphere generated by a distrubution of dipoles oriented along the axis z.

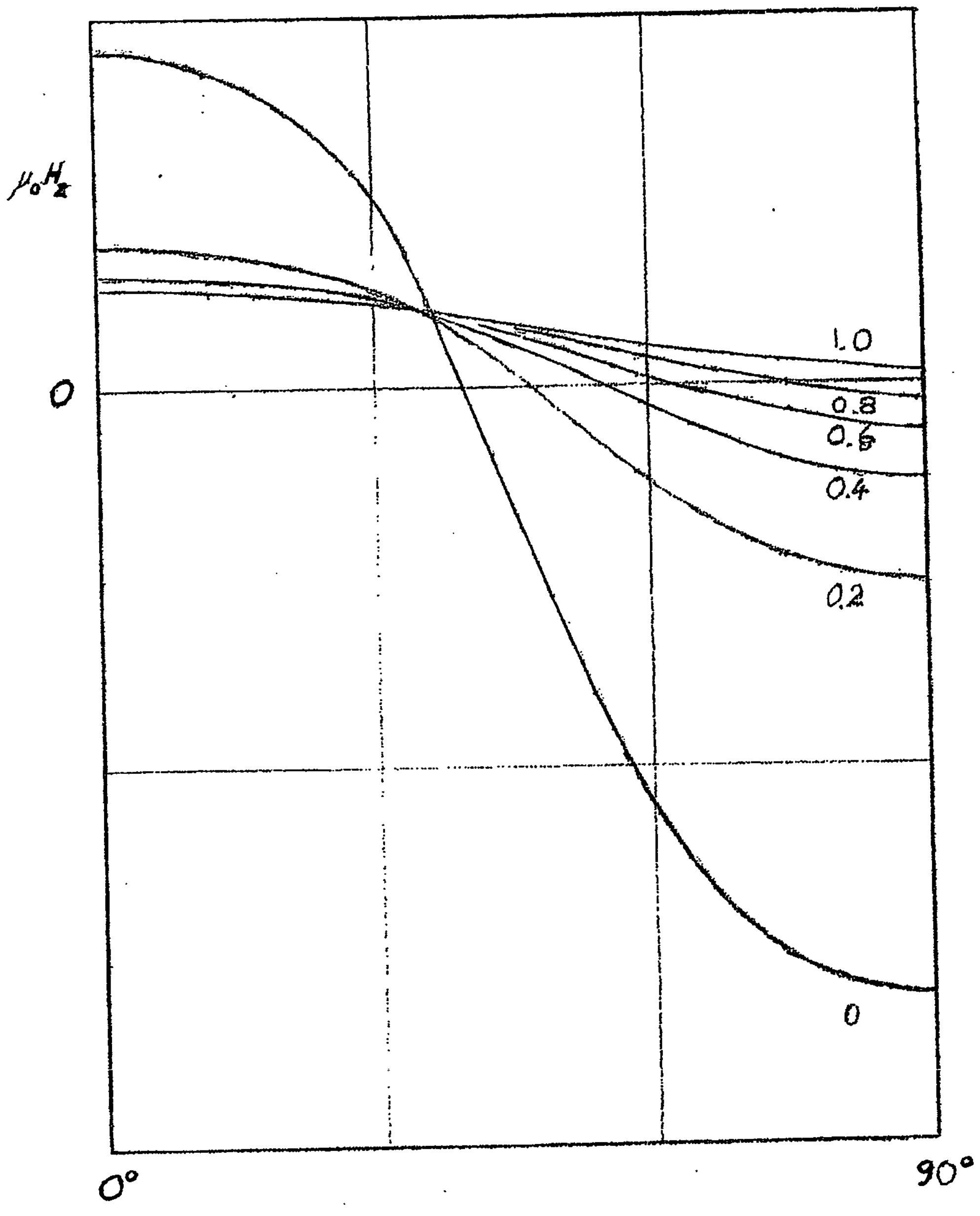

Fig. 4.4 z component of the field generated by the z component of the dipole distribution

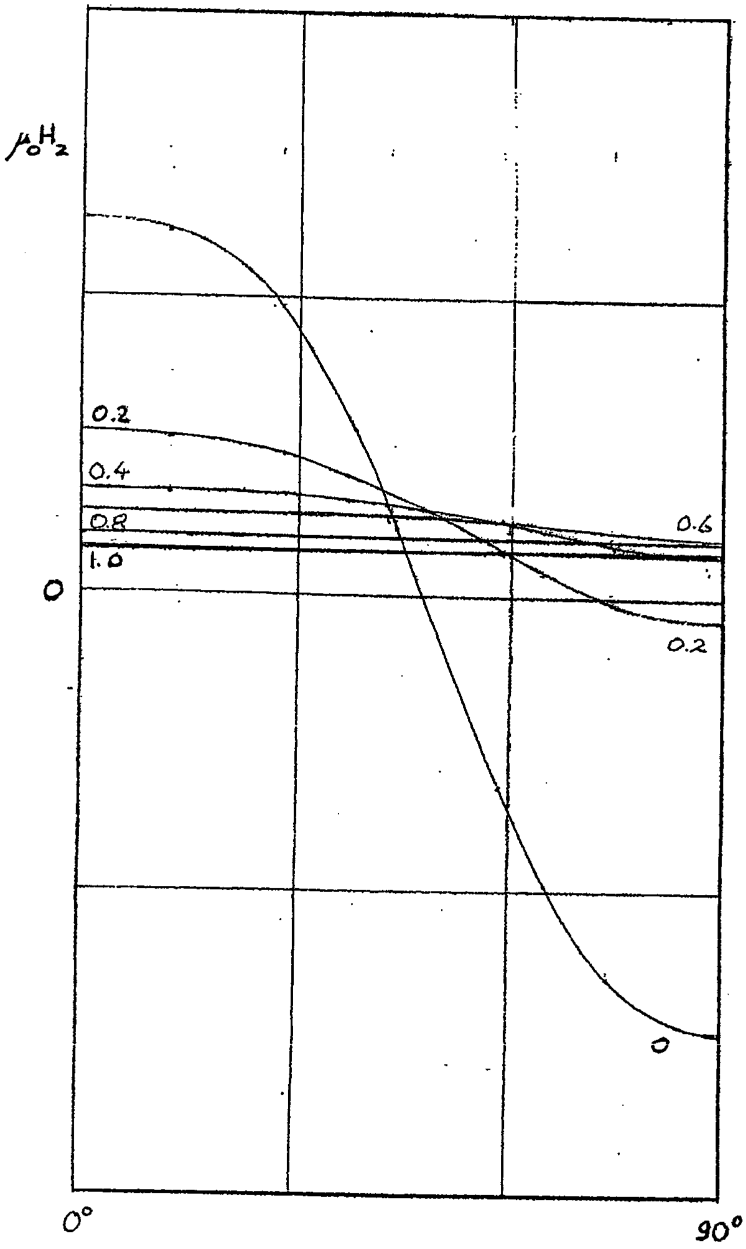

Fig. 4.5 z component of the field generated by the r component of the dipole distrubution

Where P_k is the Legendre's polynomial of the first kind defined as

$$\left\{ \begin{array}{l} P^k(x) = \frac{1}{2^k\,k!}\frac{d^k}{dx^k}\left(x^2-1\right)^k \\ x = \cos\theta \end{array} \right. \tag{4.6}$$

If the field satisfies the symmetry condition

$$H_z(\pi-\theta) = H_z(\theta) \tag{4.7}$$

the expansion (4.5) is limited to the even values of k. The coefficients b_k of the expansion are given by

$$b_k = \frac{2k+1}{2}\sum_{h=0}^{n} C_{k,h}\,p(\rho_h) \tag{4.8}$$

where

$$C_{k,h} = \int_{-1}^{+1} \Psi(\rho_h, x) P_k(x)dx \tag{4.9}$$

Identically, the distortion δ Hz of the field generated by the magnet on the reference sphere can be expanded in the spherical harmonicics

$$\mu_0\ \delta H_z(x) \ = \ \sum_{k=0}^{\infty} a_k P_k(x) \tag{4.10}$$

where the coeffecients a_k are

$$a_k = \frac{\mu_0}{2}(2_k+1)\int_{-1}^{+1}\left[\delta h_z(x)\right] P_k(x)dx \tag{4.11}$$

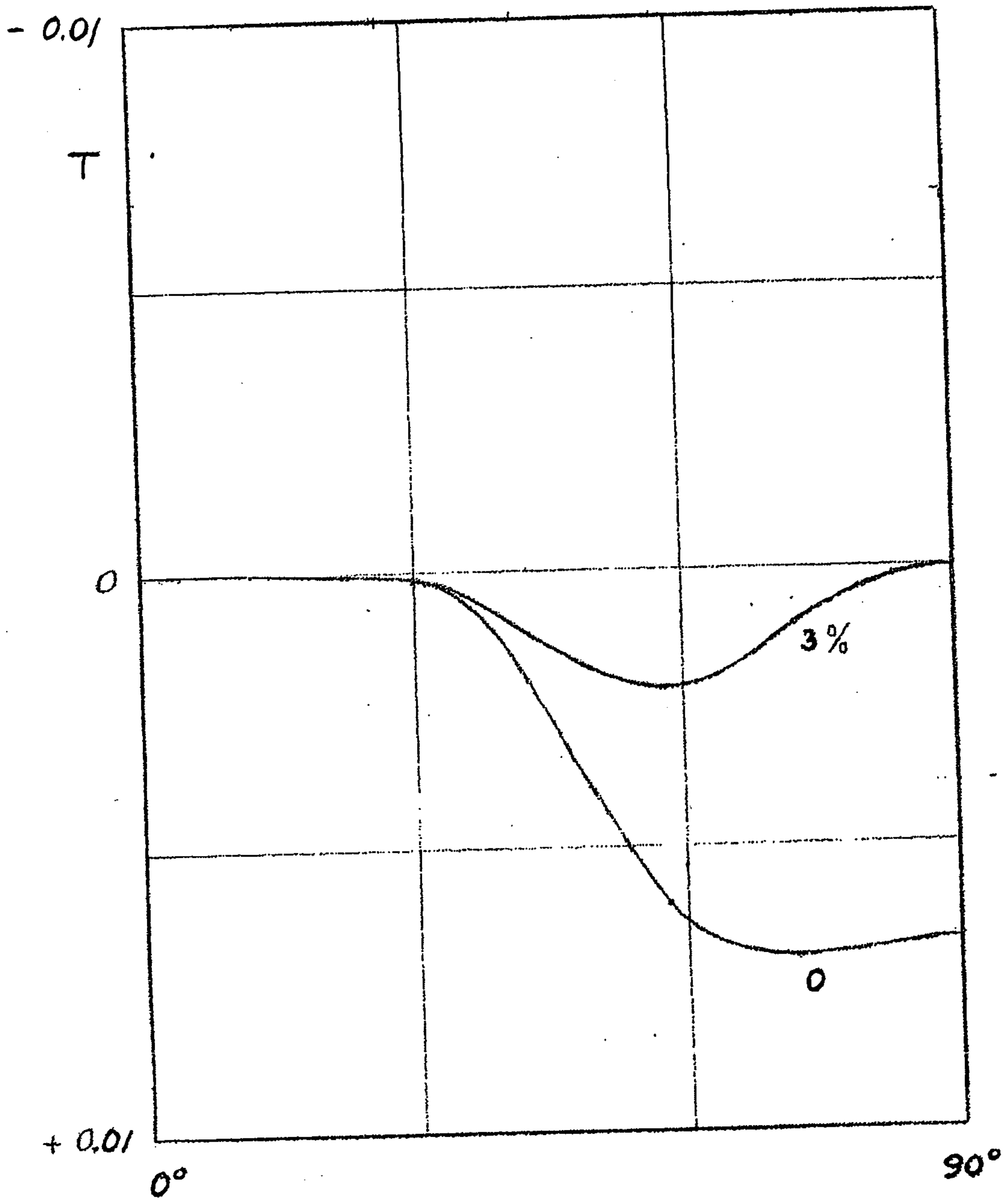

Fig. 4.6 Intensity on the reference sphere for K' = K and K' = 1.03

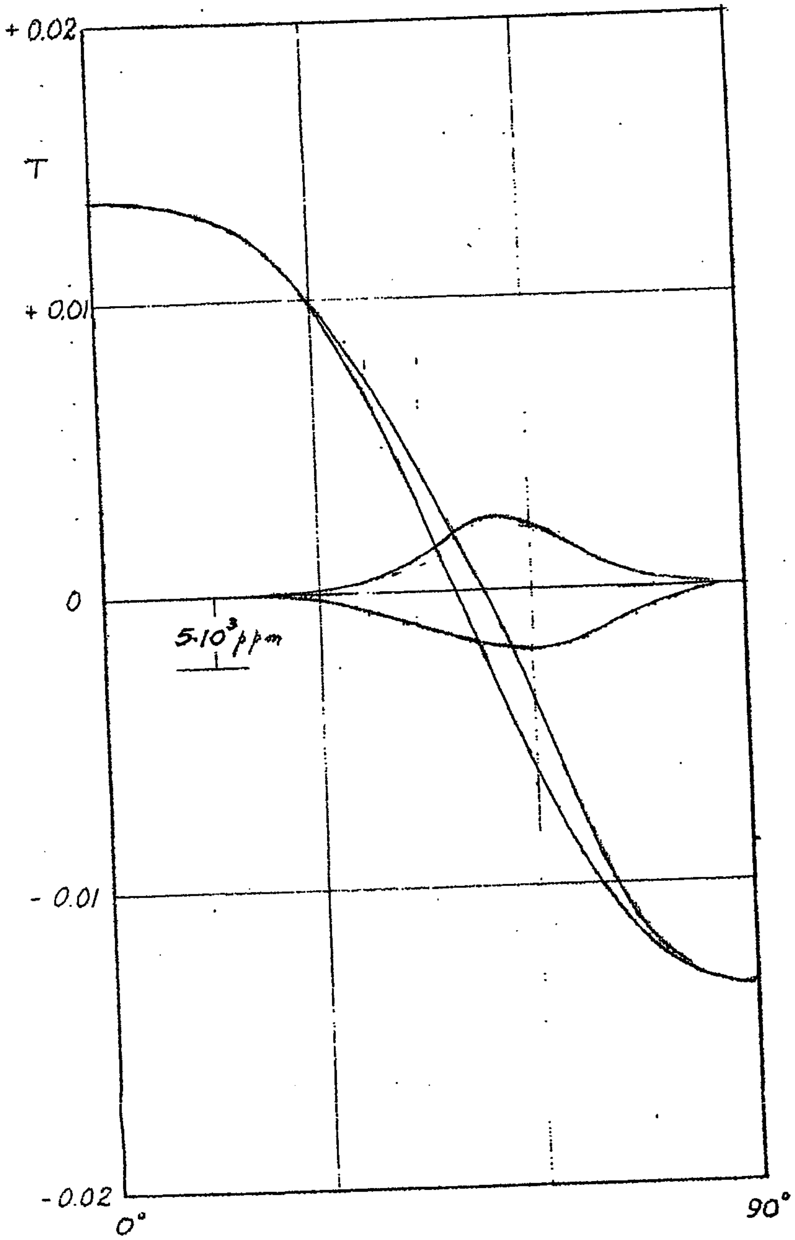

Fig. 4.7 Partial compensation of the field distortion with two dipole rings

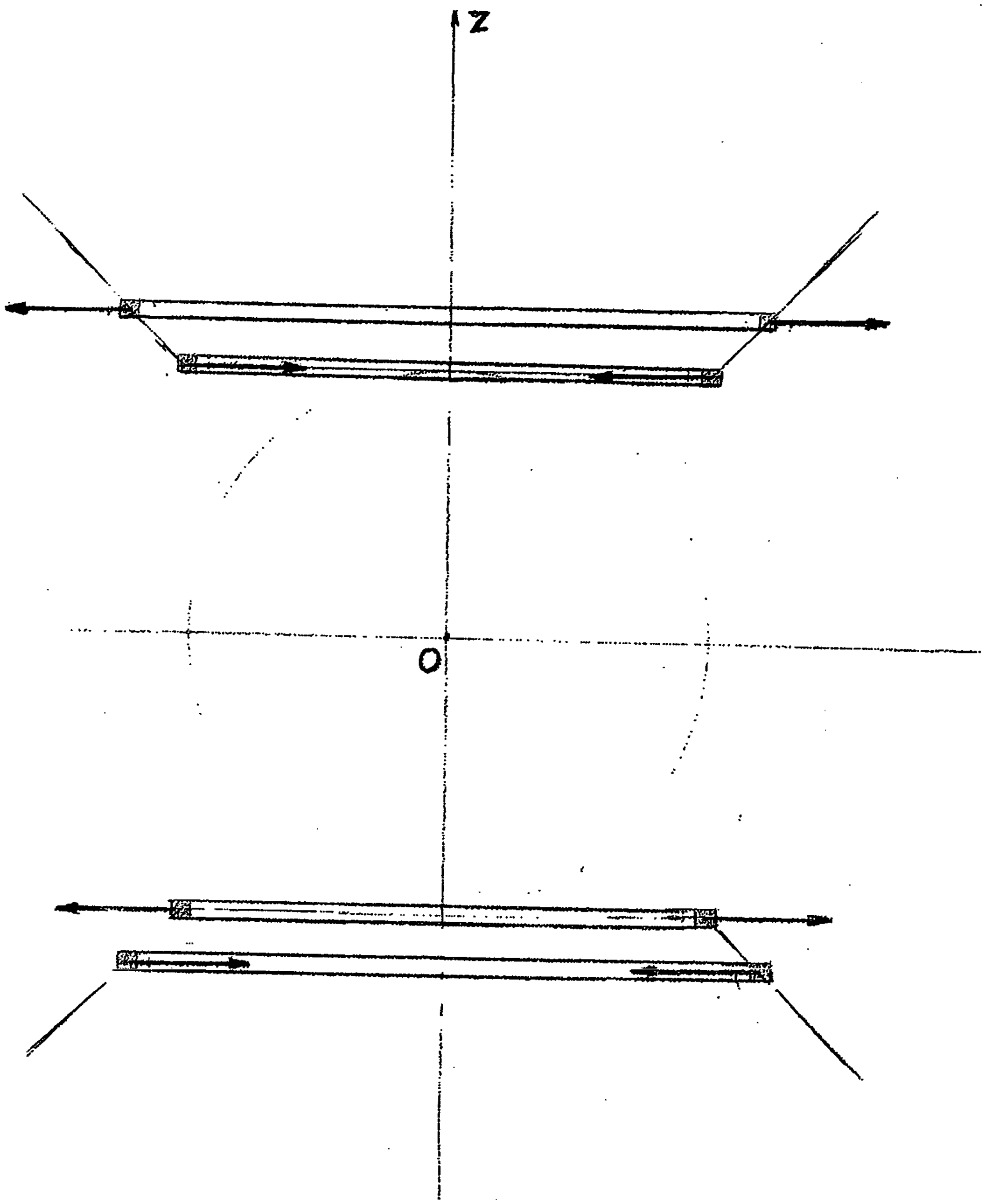

Fig. 4.8 Schematic of a two ring dipole structure

and the field distortion is eliminated if coeffiecients b_k satisfy the system of equations

$$b_k = a_k \quad (k = 0,1,2,\dots) \tag{4.12}$$

i.e. the distribution of dipoles on the conical surface $\theta = \theta_0$ that cancels the field distortion is given by the solution of the system of equations

$$\sum_{h=0}^{n} C_{k,h} \; p(\rho_h) = -\mu_0 \int_{-1}^{+1} [\delta H_z(x)] \; P_k(x)dx \tag{4.13}$$

$$(k = 0,1,2,\dots)$$

In a practical situation the compensation of the field distortion can be confined to a limited number of the lowest order harmonies, which as a consequence results in the same limited number of rings of the compensation structure of dipoles.

The compensation with the dipole distribution on the conical surface $\theta = \theta_0$ can be illustrated in the simple example of the magnetic structure introduced in Section 3 and depicted in Fig. 3.4. Consider the case of the dual distribution of magnetic material where the value of K' of the external layer in the region in larger than the value in the rest of the magnetic structure. Fig. 4.6 show the plotting of the intensity over the reference sphere for K'= K and for the optimum value (3.1) of K' which minimizes the field distortion within the sphere. A common zero level of the field in Fig 4.6 is arbitrarily chosen for the two values of K'. In the particular case of K' = 1.03K the zero level corresponds to an average value of approximately 0.47 Tesla at the center of the sphere. As shown in Fig 4.6 the field attains the same value of 0.47 Tesla at both ends of the angular integral $\theta = 0$ and $\theta = 90^\circ$. In the structure selected for the computation of Fig. 4.5, assume that the dipole distribution is limited to the first two rings, $\rho = \rho_0$, $\rho = \rho_1$ i.e.

i.e.

$$p(\rho_h) = 0 \quad h > 1 \tag{4.14}$$

Select the values of $p(\rho_0)$ and $p(\rho_1)$ that satisfy the equation

$$-p(\rho_0)\left[\Psi(\rho_0,0)-\Psi\left(\rho_0,\frac{\pi}{2}\right)\right]=p(\rho_1)\left[\Psi(\rho_1,0)-\Psi\left(\rho,\frac{\pi}{2}\right)\right] \qquad (4.15)$$

The total field generated at =0 by the two rings is

$$\mu_0\delta_1H_z(0)=p(\rho_1)\Psi(\rho_1,0)+p(\rho_0)\Psi(\rho_0,0) \qquad (4.16)$$

Thus the combination of the fields generated by the two rings over the reference sphere is the sum of a term independent of θ given by Eq. (4.16) and a second term $\delta_2H_z(\theta)$ that is zero at $\theta = 0$ and $\theta = 90^0$ and has a maximum as shown in Fig. 4.7.

The same figure shows the field generated by the two rings

$$p(\rho_0)\Psi(\rho,\theta),p(\rho_1)\Psi(\rho_1,\theta)-\theta\mu_0\delta_1H_z(0) \qquad (4.17)$$

In the first approximation the correction of the distortion is accomplished by selecting the value of the dipole moment distribution that makes the maximum of $\mu_0\delta_2H_z$ equal to the maximum of value $\mu_0\delta_2H_z$ computed in Fig 4.5 for K^1 = 1.03 K. As apparent from Fig. 4.5 the residual distortion is of the order of 10^3ppm.

The term generated by the rings does not contribute to the field distortion and its effect is a small change of the field of the magnet. A schematic of the rings configuration is presented in Fig. 4.8

5. REFERENCES

[1] Abele MG, Generation of Uniform Fields with Conical Permanent Magnets. TR 42, Department of Radiology, New York University. January 1, 1997

[2] Abele MG, Structures of Permanent Magnets, John Wiley and Sons, Inc., 1993